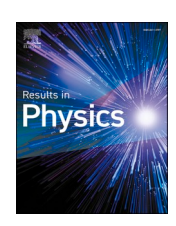
ELSEVIER

Contents lists available at ScienceDirect

Results in Physics

journal homepage: www.elsevier.com/locate/rinp





MOCVD growth and characterization of conductive homoepitaxial Si-doped Ga₂O₃

Armando Hernandez ^{a,b}, Md Minhazul Islam ^{a,b}, Pooneh Saddatkia ^{a,b}, Charles Codding ^a, Prabin Dulal ^b, Sahil Agarwal ^{a,b}, Adam Janover ^c, Steven Novak ^c, Mengbing Huang ^c, Tuoc Dang ^d, Mike Snure ^d, F.A. Selim ^{a,b,*}

- ^a Center for Photochemical Sciences, Bowling Green State University, Bowling Green, OH 43403, USA
- ^b Department of Physics and Astronomy, Bowling Green State University, Bowling Green, OH 43403, USA
- ^c College of Nanoscale Science and Engineering, State University of New York Polytechnic Institute, Albany, NY 12203, USA
- ^d Air Force Research Laboratory, Sensors Directorate, Wright Patterson AFB, OH 45433, USA

ARTICLE INFO

Keywords: Metal organic chemical vapor deposition Thin films Semiconductors Electrical properties SIMS Thermoluminescence

ABSTRACT

Epitaxial Ga_2O_3 films were grown by Metal Organic Chemical Vapor Deposition (MOCVD) on native substrates at growth rate of 1 μ m/hour. The electron conductivity was introduced in the films through Si doping during deposition and the growth and doping parameters were optimized to control the electrical transport properties. The films were characterized in terms of structure, surface morphology, electrical transport properties, dopant concentrations and trapping defects. It was found that electron densities are not solely dependent on dopant concentrations and the use of metal organic precursor seems to induce additional donors of carbon. The work shows that the electron density and conductivity of MOCVD Ga_2O_3 films are mainly governed by the interplay between dopant concentration, C concentration and the presence of trapping defects in the films, which is most likely applicable for other oxide films grown by MOCVD. Conductive films of Ga_2O_3 with resistivity in the order of $0.07~\Omega$.cm were successfully grown. The electron density in most of these films was in the range of $10^{19}~cm^{-3}$ but the mobility was limited to $1.5~cm^2/V$ -s. Higher mobility of $30~cm^2/V$ -s was obtained in some films at the expense of carrier concentration by reducing Si doping level resulting in resistivity in the order of $0.3~\Omega$.cm. This range of conductivity and mobility is relevant for field-effect transistors (FET) and the applications of Ga_2O_3 as transparent FET in Deep Ultra-Violet (DUV) technology.

Introduction

Gallium oxide (Ga_2O_3) has attracted much attention as a potential oxide semiconductor for high power devices, photodetectors, and other applications due to its ultra-wide band gap and high breakdown voltage [1–6]. Furthermore, our recent development of highly p-type and n-type conductive Ga_2O_3 [7] opens more possibilities for Ga_2O_3 based devices and applications. Unlike SiC and GaN, which are also candidates for high power devices, large size β -Ga $_2O_3$ bulk substrates can be grown by different melt growth methods making Ga_2O_3 homoepitaxial growth very affordable. Fortunately, several growth techniques such as Czochralski method (CZ) [8,9], floating zone (FZ) [10,11] and edge-defined film fed (EFG) [12] were successfully adopted to grow bulk β -Ga $_2O_3$ substrates. β -Ga $_2O_3$ is highly insulating in its defect free form, however, Si and Ir atoms from the β -Ga $_2O_3$ seed and crucible often lead to

unintentionally doped (UID) n-type conductivity in the material [12]. Deep acceptors like Mg and Fe are commonly used to compensate those n-type dopants to achieve the semi-insulating property [13]. High purity thin films with high carrier concentration and good mobility need to be realized for the successful development of devices. However, epitaxial growth of thin films often faces many challenges when attempting to minimize defects in the lattice and control dopants. Recently, several epitaxial growth methods have been employed to grow $\beta\text{-}Ga_2O_3$ thin films and electron concentration ranging from 10^{16} to 10^{19} cm $^{-3}$ has been reported for doped thin films grown by Molecular Beam Epitaxy [14], and metal organic chemical vapor deposition (MOCVD) [15,16,17]. Earlier, Gogova et al. [18] reported the growth of Si doped $\beta\text{-}Ga_2O_3$ on sapphire (0001) substrate by MOVPE method and the films were n-type with electron concentrations in the range from 10^{16} cm $^{-3}$ to 10^{18} cm $^{-3}$.

^{*} Corresponding author at: Center for Photochemical Sciences, Bowling Green State University, Bowling Green, OH 43403, USA. *E-mail address:* faselim@bgsu.edu (F.A. Selim).

A. Hernandez et al. Results in Physics 25 (2021) 104167

MOCVD technique, which is the growth method employed in this work exhibits excellent reproducibility and can be scaled up for high volume production [19]. Recently, the rotating disc MOCVD reactor has been used by Sbrockey et al. to achieve large area growth of $\beta\text{-}Ga_2O_3$ films [20], while Alema et al. investigated the growth of $\beta\text{-}Ga_2O_3$ epitaxial films using a close coupled showerhead MOCVD [21]. Takiguchi et al. showed that epitaxial films can be grown by low temperature MOCVD using trimethyl gallium and water [22] and Lv et al. studied the epitaxial relationship between $\beta\text{-}Ga_2O_3$ and sapphire substrates [19]. Recently, density functional theory and molecular dynamics studies have became very useful to understand the correlation between the MOCVD growth conditions and the structural and electronic properties of the films [23–24].

In this work, we study the growth of homoepitaxial β-Ga₂O₃ films doped with Si using close coupled showerhead MOCVD technique and vary the ratio of gallium/oxygen and silicon precursor to produce conductive epitaxial films. Then, we characterize the films in terms of structure, surface roughness, electrical transport properties, dopant concentrations, and trapping defects and demonstrate the effect of precursor mass flow rates and dopant concentrations on the film properties. The study reveals the strong interplay between the growth parameters, dopant concentrations and defects in the films. By the right tuning of growth parameters, films with relevant electrical transport properties for applications of Ga₂O₃ in field-effect transistors (FET) in high power and deep ultra-violet (DUV) transparent devices can be realized. Ga₂O₃ has been already recognized as a potential semiconductor for novel DUV technology [25-28]. Matsuzaki et al. recently described how the electrical properties of DUV transparent Ga₂O₃ films must sustain a conductivity value less than 7×10^{-3} S/cm assuming a drift 'mobility of $\sim 0.44 \text{ cm}^2/(\text{V} \cdot \text{s})$ to attain proper functionality of FETs [29]. These values can be easily realized and controlled through the growth process and parameters reported here.

Description of BGSU's MOCVD system

Bowling Green State University's MOCVD is an Agnitron system with a few modifications. It uses a closed coupled showerhead technique that allows chemicals to be introduced vertically into the reaction chamber. The showerhead is designed for an equal distribution of gaseous precursors throughout the chamber onto the wafer. The showerhead is located approximately 15 cm above the heated wafer to allow for a quick, uniform diffusion of gas molecules onto the rotating, heated wafer. A schematic diagram for the reaction chamber is shown in Fig. 1.

The wafers are placed on a carrier that can rotate up to 1000 rpm. A resistance heater is isolated beneath the carrier to adjust the temperature from RT to 1000 °C. Fig. 1 illustrates how the precursors and gases are introduced to the shower head and the reaction chamber. Nitrogen gas is used for purging the system and argon is used as a gas carrier for the metal organic precursors. The system uses a turbomolecular-pump (EBARA) to generate many degrees of vacuum from intermediate vacuum ($\sim 10^{-2}$ Pa) up to ultra-high levels ($\sim 10^{-8}$ Pa) inside the reaction chamber giving the gas molecule a preferential diffusion vacuum. A high velocity water stream flows over the walls of the chamber to prevent over heating of the reaction chamber. Lines carrying the precursors in the system are wrapped with heating tapes to prevent deposition inside them and minimize cross contamination. The metal organic precursors are stored in bubblers kept at relevant temperatures according to their vapor pressure. A large number of atomic precision mass flow rate controllers are used to adjust the flow rates of the precursors and gases through the system. The system is fully controlled by Imperium software from Agnitron technologies.

Ga₂O₃ growth parameters and conditions

Undoped and doped Ga_2O_3 films were epitaxially grown on semi-insulating substrates of (010) CZ β - Ga_2O_3 single crystal. Metal organic trimethyl-gallium (TMG) and oxygen were used as precursors and 40 ppm silane (SiH₄)/He gas mixture was used for doping. The TMG

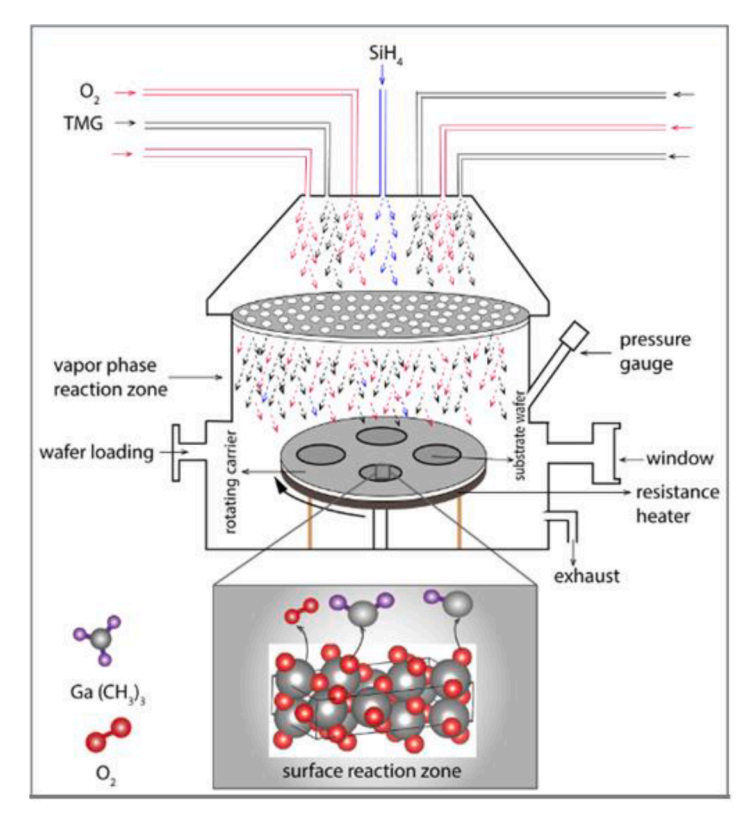


Fig. 1. A Schematic diagram showing the MOCVD reaction chamber.

bubbler was kept at -10 °C during the growth process.

Before each growth, the parameters were selected, and a recipe is created and inserted into the IMPERIUM software. The film thickness is mainly controlled by deposition time and growth rate, which is strongly affected by the growth pressure in the chamber, substrate temperature, and precursor flow rate. The growth rate here is about 1 $\mu m/hr$. For all films reported here, the substrates were heated to 740 °C, rotated at 750 rpm and pure molecular oxygen (5 N) was separately injected into the reactor to mix with the TMG precursors for oxidation with oxygen flow rate of 1800 sccm. Before growth, Ga_2O_3 substrates were degreased using ethanol, isopropanol, and deionized water by ultrasonic bath and then dried with N_2 . Once the carrier is loaded with substrates in place, the chamber is pumped down, and the growth commences. Steps are carried out following the recipe and fully executed by the software.

Characterization methods

A. Hernandez et al.

X-ray diffraction (XRD) measurements were performed using a Rigaku diffractometer [30] and the XRD patterns of $\rm Ga_2O_3$ films were analyzed using PDXL software (Rigaku). The surface morphology of the films was investigated by atomic force microscopy (AFM) [31]. Hall-effect measurements were performed using an MMR Hall-effect system and Van der Pauw Hall effect measurements were used to determine sheet resistance, carrier density and hall mobility at room temperature. Four indium contacts were made in a square arrangement on the samples, and the contact area was kept as small as possible. The measurements were performed at a constant magnetic field of 9300 G. Secondary Ion Mass Spectrometry (SIMS) measurements were carried out using a PHI 6650 quadrupole-based SIMS instrument. Profiles were acquired using 5 keV Cs + bombardment at an incidence angle of 60° from normal and the secondary ions were detected.

Thermal stimulated luminescence (TSL) measurements were carried out on the most resistive sample via a spectrometer that was developed by one of the authors and described in detail elsewhere [32–35] allowing for a direct measurement of the luminescence as a function of both wavelength and temperature. First the sample was irradiated with UV light in dark at liquid nitrogen temperature of 77 K. Then after irradiation, the sample was linearly-ramp heated to 400 °C at a rate of 60 °C/min and the corresponding luminescent spectrum was recorded from 200 to 800 nm using a charge-coupled device detector.

Results and discussion

The as-grown films were studied by several characterization techniques to determine the structure, surface roughness, dopant concentrations and electrical properties. X-ray Diffraction (XRD) results in Fig. 2 confirm the formation of β-Ga₂O₃ phase with a preferred orientation along the (010) direction as shown from the peak around 60°. Comparing the film XRD with the diffraction pattern of the substrate showed that the film orientation is aligned with the substrate and the peak is more intense and sharper for the film. The XRD peak position for each film is shown in Fig. 2. There is a small shift to the left in the peak of most of the doped films at (60.4) compared to the undoped sample #3 (61.2) due to the incorporation of Si atoms in Ga₂O₃ lattice and the significant difference between the size of Si atom and Ga atom. Higher doping led to a relatively bigger shift in the peak position. The difference in the FWHM of XRD peaks indicated in Fig. 2 illustrate the effect of doping and changing the mass flow control rate of precursors on the crystal quality. The morphology and surface roughness of one resistive and one conductive film were studied by Atomic Force Microscopy (AFM) and presented in Fig. 3, which reveals a rough surface for the two films. This roughness did not hinder the conductivity as indicated from the electrical transport measurements of sample # 9 shown below. Nevertheless, it is well known that high roughness would impact the performance of devices and it should be better controlled for device studies. However, our study here only focused on understanding the

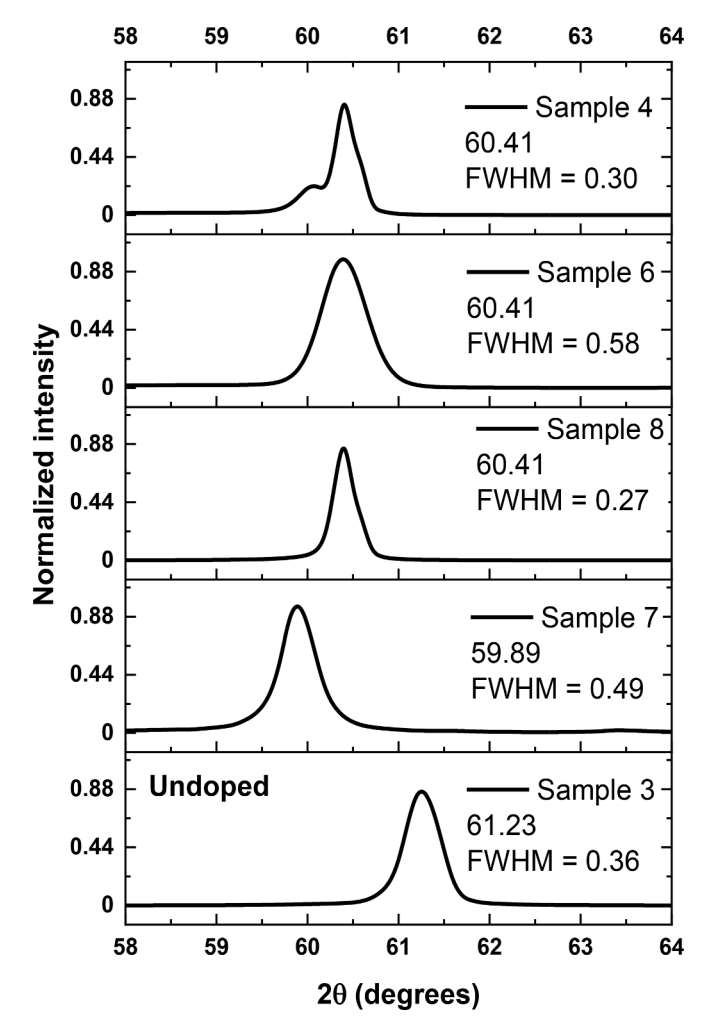


Fig. 2. XRD measurements for undoped and Si-doped β -Ga $_2$ O $_3$ films grown with different mass flow rates of TMG.

relation between the growth conditions, dopants, trapping defects and electrical properties.

The mass flow rates of TMG and SiH₄ were varied to determine the optimal growth conditions to attain high carrier concentration. Table 1 summarizes the electrical parameters of the films as well as the mass flow rates of TMG and Silane. The mass flow rates of TMG and silane vary from 31.3 to 93.8 µmol/min and from 0 to 89.2 nmol/min, respectively. The sheet resistance and sheet carrier concentration of the films were also plotted in Fig. 4 as function of the mass flow rates for TMG and Silane. The table and figures show that the sheet resistance of the films covers a wide range from 1.33×10^3 to 3.22×10^9 Ω cm⁻². It should be mentioned that the substrates are highly resistive and could not be measured by our Hall-effect system which can measure up to 10^{12} Ω cm⁻². Sample 9 grown with 49.1 µmol/min TMG and 89.2 nmol/min silane exhibits the lowest sheet resistance and highest sheet carrier concentration. The same conditions were repeated for sample 6, which also exhibits high conductivity and very close sheet resistance and carrier sheet number values indicating the reproducibility of the results and confirming that these growth parameters are relevant for producing conductive films. It can be seen from Table 1 that the lower Si concentration of 8.92 and 17.8 nmol/min led to the highest electron mobility of about 30 cm²/V·s. Increasing the concentration of Si dopants significantly increased the sheet electron number up to $3x10^{15}\ cm^{-2}$ which gives sheet resistance of $10^3 \Omega/cm^2$ but reduces the mobility by one order of magnitude. This implies that incorporation of Si atoms enhances scattering of charge carriers reducing their mobility. Indeed, the

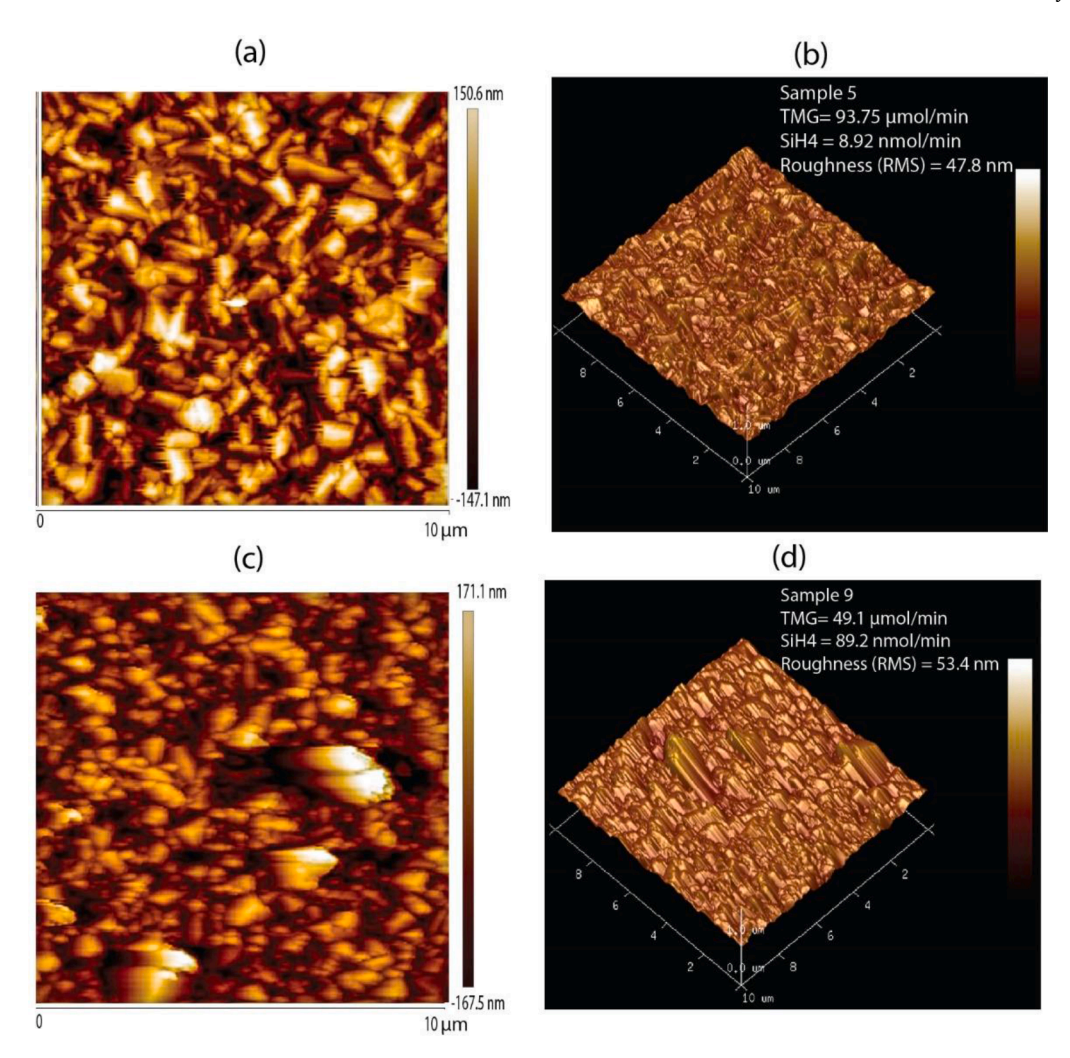


Fig. 3. AFM images of: very resistive film (a, b) and most conductive film (c, d), their RMS surface roughness is 47.8 nm and 53.4 nm.

Table 1 Growth conditions and electrical transport properties of Si doped ${\rm Ga_2O_3}$ films.

Sample Name (TMG: SiH4).	O/Ga Ratio	SiH ₄ (nmol/ min)	TMG Flow rates (µmol/ min)	Sheet Resistance (Ohm/cm ²)	Sheet Number (cm ⁻²)	Mobility (cm ² /Vs)
Sample 1	$\begin{array}{c} 7 \times \\ 10^4 \end{array}$	8.92	49.1	1.78E + 05	4.85E + 12	2.90E + 01
Sample 2	$\begin{array}{c} 7 \times \\ 10^4 \end{array}$	17.8	49.1	4.44E + 04	1.61E + 13	3.09E + 01
Sample 3	$\begin{array}{c} 7 \times \\ 10^4 \end{array}$	0	49.1	$>10^{12}$	N/A	N/A
Sample 4	3.9 × 10 ⁴	89.2	93.8	1.19E + 04	4.16E + 14	1.51E + 00
Sample 5	3.9 × 10 ⁴	17.8	93.8	1.37E + 09	8.05E + 06	N/A
Sample 6	$\begin{array}{c} 7 \times \\ 10^4 \end{array}$	89.2	49.1	5.64E + 03	1.95E + 15	5.85E-01
Sample 7	$^{1\times}_{10^5}$	89.2	31.3	3.22E + 09	2.90E + 06	N/A
Sample 8	8.7 × 10 ⁴	89.2	40.2	2.78E + 05	1.05E + 13	2.53E + 00
Sample 9	$\begin{array}{c} 7\times\\ 10^4\end{array}$	89.2	49.1	1.33E + 03	2.95E + 15	1.59E + 00

carrier mobility in Ga_2O_3 and semiconductors in general is highly impacted by doping. Doping increased the scattering due to the formation of ionized impurities acting as donors and the formation of defects associated with dangling bonds.

The undoped sample shows very high resistivity more than 10^{12} Ω/cm^2 (the sensitivity of our Hall measurement system). This high resistance implies that the films do not contain significant background of intrinsic/extrinsic shallow donor defects. One important observation from Table 1 and Fig. 4 is that the dopant flow rate does not solely determine the conductivity of the films. SIMS was performed on 4 films to measure the actual Si concentrations incorporated in the films and Fig. 5 a depicts the depth resolved Si concentration for films grown with different TMG flow rates but same silane flow rate of 10 sccm. The films show plateaus of close or similar concentration of silicon, but different thickness as expected due to different TMG flow rates and growth time. The Si concentration measured within the plateau is in the order of 10^{19} cm⁻³ for all films and only varied from (3.0 to 5.4) \times 10¹⁹ cm⁻³. The thickness of the films was approximately determined from the depth where silicon concentration decreases abruptly indicating the substratefilm interface. Carbon is a common impurity in MOCVD growth because of the use of metal organic precursors and it may affect the electrical properties of the films or the formation of complex defects in them. Thus, it is important to determine its concentrations in Ga₂O₃ films. The level of carbon impurity in the films is measured by SIMS and depicted in Fig. 5 (b). It can be seen from the figure that the carbon contamination is highest on the surface and decreases rapidly with the film depths and it does not exhibit a clear plateau as in the case in Si which indicates that C

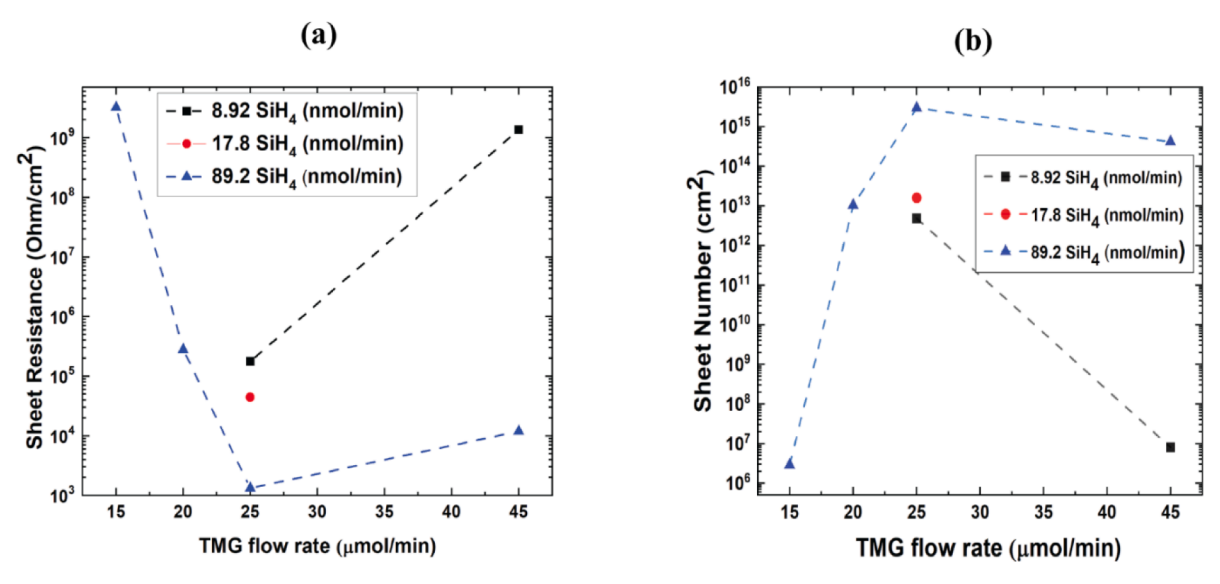


Fig. 4. The sheet resistance (a) and sheet carrier number (b) as a function of the mass flow rate of Ga and Si precursors.

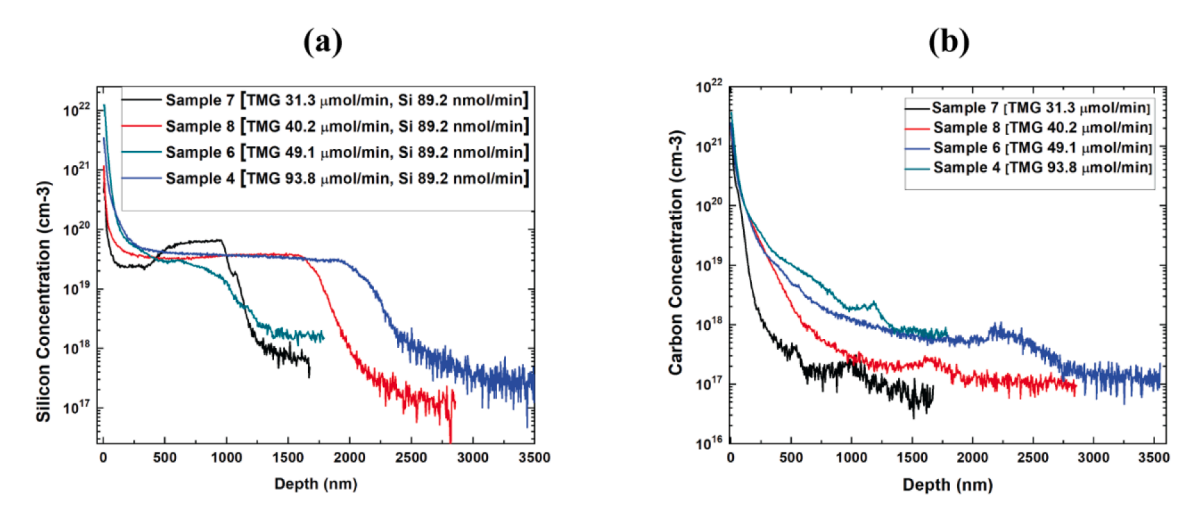


Fig. 5. SIMS results: depth resolved silicon concentration (a) and carbon concentration (b) in Ga₂O₃ films grown with different oxygen/gallium (O/Ga) ratio.

mainly diffuses to the films after growth and does not incorporate in the structure during layer deposition. Obviously, the carbon level is dependent on the TMG flow rate which is illustrated in Fig. 5 (b) and Table 2. C can incorporate as an interstitial close to O atoms and form C-

 $\label{eq:continuous} \textbf{Table 2} \\ \textbf{Silicon and carbon concentrations in correlation with the resistivity and carrier density of Si doped Ga_2O_3 films. The table also displays the O/Ga growth ratio for each film.} \\$

Sample Name (TMG/ SiH4)	Si conc. (cm ⁻³) at 600 nm	Carbon conc. (cm ⁻³) at 1400 nm	Film thickness (nm)	Resistivity (Ω. cm)	Carrier density cm ⁻³	O/Ga Ratio
Sample 6	3.98E + 19	6.92E + 17	624	3.52E-01	3.13E + 19	7 × 10 ⁴
Sample 4	3.07E + 19	7.79E + 17	1943	2.31E + 00	2.14E + 18	3.9 × 10 ⁴
Sample 8	3.14E + 19	2.04E + 17	1629	4.53E + 01	6.44E + 16	8.7 × 10 ⁴
Sample 7	5.42E + 19	8.23E + 16	956	3.08E + 05	3.03E + 10	$\begin{array}{c} 1\times\\10^5\end{array}$

O bonds, always acting as a shallow donor because only its positive charge states are stable over the entire band gap [36]. C on the Ga site is more stable on the tetrahedral site; but moves off the Ga site and also forms C-O bonds. The +charge state is most stable providing a shallow donor. Thus, C would exclusively act as a shallow donor in Ga_2O_3 .

Table 2 presents the Si concentration, C concentration, thickness of each film compared with the carrier density calculated from the sheet carrier number and the thickness. It also includes the resistivity and O/ Ga growth ratio for each film to facilitate the discussion. All films have lower carrier density than Si concentrations even in the most conductive films. Careful inspection of the data shows that sample 7 has the highest Si concentration but the lowest carrier density and highest resistivity. However, Fig. 5 reveals that the Si concentration in this sample is lower than the other films in the first 500 nm. Sample 8 has higher Si concentration than sample 4 but 2 orders magnitude less carrier density. This large discrepancy between the carrier density and Si concentration implies that there are other factors affecting the formation of charge carriers in the films besides Si. As discussed above C impurities also influence the film transport properties and act as shallow donors and sample 7 and 8 have indeed the lowest carbon concentration. However, the difference in carbon concentration between films is small and cannot account for the large difference in carrier density. In addition, the undoped films are always highly resistive despite the expected presence

A. Hernandez et al. Results in Physics 25 (2021) 104167

of carbon in them. Accordingly, we anticipate that carbon may have small effect on the carrier density only in doped films probably because of the formation of more stable carbon related defects acting as donors.

An important difference between the resistive samples 7 and 8 and the conductive samples 4, 6 and 9 is the O/Ga growth ratio which can greatly impact defect types and concentrations in the films. This ratio is higher in the resistive films; Sample 7 is the most resistive sample by far has the highest O/Ga ratio. High O/Ga ratio results in Ga poor phase and the formation of Ga vacancies which are known to be deep acceptors in Ga₂O₃ [37-40]; compensating Si donors. This can explain the reason behind the high resistivity in this sample. However, if we compare O/Ga ratio in the conductive films 6 and 4, this argument does not hold. Sample 6 has higher carrier density and higher O/Ga ratio than sample 4 (although the difference in carrier density is not large). The lower carrier density in sample 4 may be due to the lower concentration of Si in the sample. From the aforementioned discussion, the electrical transport of the films cannot be simply correlated to one parameter such as the dopant concentrations or the presence of deep acceptors. They are rather consequences of the interplay of several factors including dopant concentration, impurity concentration and the presence of deep acceptors.

The strong dependence of the transport properties on the combined effect of these factors is expected to dominate in all oxide films grown by MOCVD. In our discussion we predicted the formation of deep acceptors of Ga vacancies from the O/Ga growth condition, however, it is also important to consider other possible origins of deep acceptors in the films such as other Ga vacancy related defects or Fe impurities which may diffuse from the semi-insulating Ga₂O₃ substrate to the film.

To further investigate the presence of deep acceptors in Si doped Ga_2O_3 , we carried out TSL spectroscopy on a resistive film. In previous works, we have established TSL as an effective method of detecting both shallow and deep traps in oxides, dielectrics, and semiconductors [41–43] including Ga_2O_3 single crystals and films [2,44]. In fact, we recently showed that TSL can be used to calculate the concentration of compensating acceptors in Ga_2O_3 [45]. Thus, TSL measurements here may give some indication about the presence and number of different types of deep acceptors in the resistive films. Fig. 6 displays the 3-dimensional TSL emission as a function of temperature and wavelength (Fig. 6a) with its projection on x-y plane showing the contour plot (Fig. 6b) and its glow curve calculated from integrating the emission over the whole range of wavelength (Fig. 6c). The figures show a strong

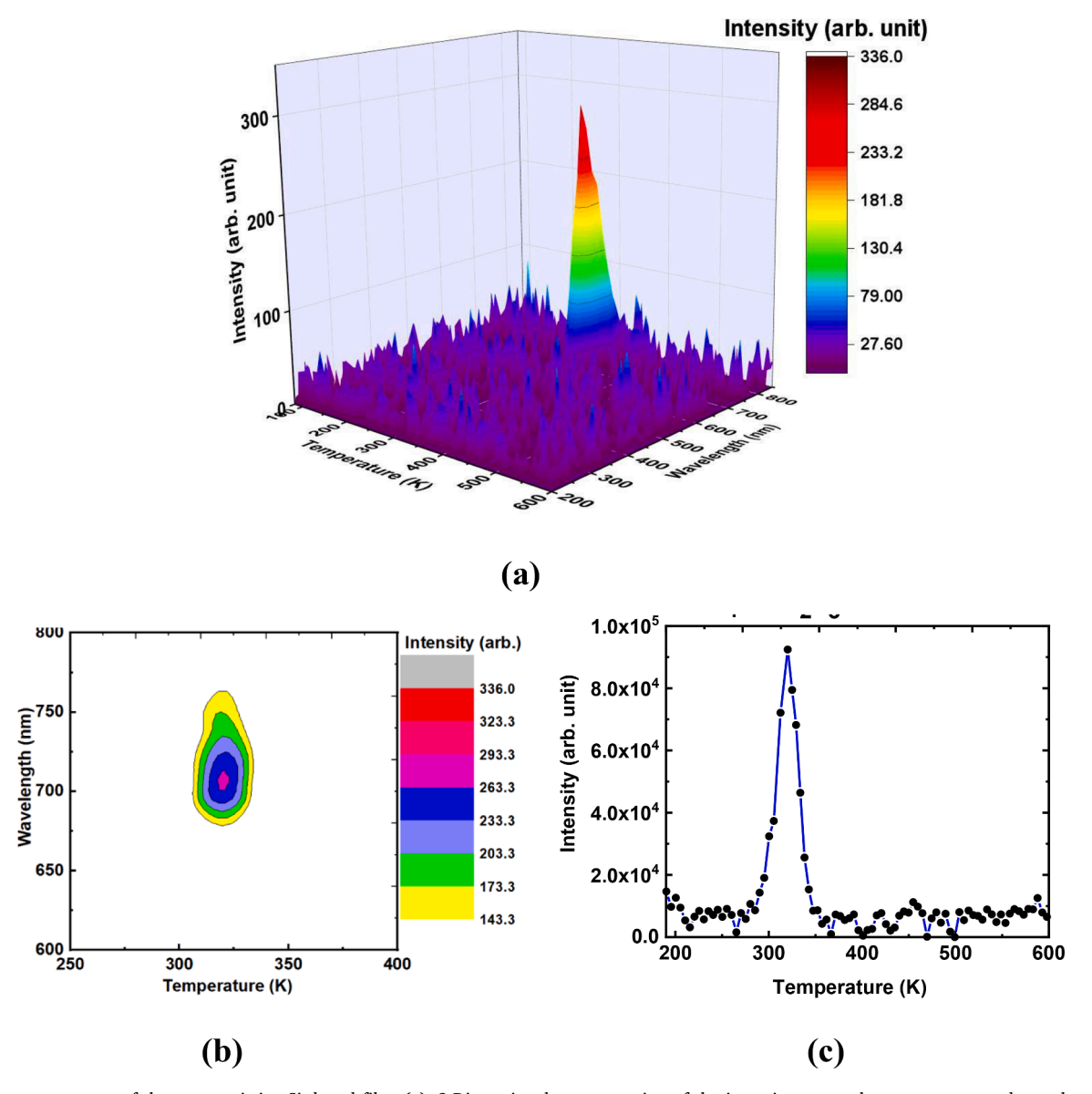


Fig. 6. TSL measurements of the most resistive Si doped film. (a): 3-Dimensional representation of the intensity versus the temperature and wavelength, (b): its contour plot, (c): TSL glow curve obtained from the integration of emission over the entire wavelength at each temperature.

A. Hernandez et al. Results in Physics 25 (2021) 104167

peak around 320 K illustrating the presence of deep traps which can act as compensating acceptors in n-type films. There is also a shoulder around 300 K in the peak (Fig. 6c) illustrating the presence of another trap. These measurements thus suggest there are more than one type of defects acting as trapping centers for electrons in the films and explain the reason behind the low carrier concentrations and high resistivity in some films. The wavelength emission is peaking around 700 nm (Fig. 6 a) and Fig. 6b) and spreading over 100 nm suggesting broad emission most likely associated with more than one impurity or defect center. The 700 nm emission is common in most oxides and it has been shown to be associated with small levels of Fe impurities [46]. The measured TSL glow curve and the emission wavelength together with the O/Ga ratio and the electrical measurements confirm the presence of both Gavacancies and Fe impurities and their strong roles as compensating acceptors in these films.

Conclusions

Homoepitaxial conductive Si doped β-Ga₂O₃ thin films were successfully grown at high growth rate of 1 µm/hr by MOCVD in a closed coupled showerhead vertical rotating system. The optimal process parameters were determined by varying the dopant and metal organic precursor mass flow rates. The electrical transport properties of the films were found to be governed by the interplay between dopant concentration, carbon concentration and trapping defects. This finding is expected to be true not only in Ga₂O₃ but in all oxide films grown by MOCVD. A wide range of resistivity from 3.08E + 05 to 7.0E-02 Ω .cm and carrier density from 3.0E + 10 to 5.0E + 19 cm⁻³ was measured in the films. Conductive films with less than 0.1 $\Omega.\text{cm},\,10^{19}\,\text{cm}^{-3}$ electron density and 1.5 cm²/V·s mobility and films with 2.0 Ω .cm sheet resistance and 30 cm²/V·s mobility were successfully fabricated. This range of conductivity should be relevant for field effect transistors (FETs) and application of Ga₂O₃ as transparent FETs in deep ultraviolet (DUV) technology. Moreover, the high growth rate creates an opportunity of low cost and low energy consuming production of the films.

CRediT authorship contribution statement

Armando Hernandez: Investigation, Data curation, Visualization, Writing - original draft. Md Minhazul Islam: Investigation, Data curation, Visualization. Pooneh Saddatkia: Investigation. Charles Codding: Investigation, Resources. Prabin Dulal: Investigation. Sahil Agarwal: Investigation, Visualization. Adam Janover: Investigation, Data Curation, Visualization. Steven Novak: Investigation, Data curation. Mengbing Huang: Investigation, Visualization. Tuoc Dang: Investigation, Visualization. F.A. Selim: Conceptualization, Project administration, Resources, Writing - review & editing.

Declaration of Competing Interest

The authors declare that they have no known competing financial interests or personal relationships that could have appeared to influence the work reported in this paper.

Acknowledgement

This work is supported by the National Science Foundation (NSF) under grant number DMR-2005064.

References

- [1] Baldini M, Galazka Z, Wagner G. Recent progress in the growth of β-Ga2O3 for power electronics applications. Mater Sci Semicond Process 2018;78:132–46.
- [2] Saadatkia P, Agarwal S, Hernandez A, Reed E, Brackenbury ID, Codding CL, et al. Point and extended defects in heteroepitaxial β– G a 2 O 3 films. Phys Rev Mater 2020;4(10):104602.

[3] Wang Q, Chen J, Huang P, Li M, Lu Y, Homewood KP, et al. Influence of growth temperature on the characteristics of β -Ga2O3 epitaxial films and related solarblind photodetectors. Appl Surf Sci 2019;489:101–9.

- [4] Wang Q, Huang P, Liu Q, Li Y, Qu Q, Li M, et al. Ultra-wide-bandgap (ScGa) 2O3 alloy thin films and related sensitive and fast responding solar-blind photodetectors. J Alloy Compd 2020;834:155036.
- [5] Huso J, McCluskey MD, Yu Y, Islam MM, Selim F. Localized UV emitters on the surface of β-Ga₂O₃. Sci Rep 2020;10:21022. https://doi.org/10.1038/s41598-020-76967-6.
- [6] Tadjer MJ, Mahadik NA, Wheeler VD, Glaser ER, Ruppalt L, Koehler AD, et al. A (001) β-Ga2O3 MOSFET with 2.9 V threshold voltage and HfO2 gate dielectric. ECS J Solid State Sci Technol. 2016;5(9):468.
- [7] Islam MM, Liedke MO, Winarski D, Butterling M, Wagner A, Hosemann P, et al. Chemical manipulation of hydrogen induced high p-type and n-type conductivity in Ga 2 O 3. Sci Rep 2020;10:6134.
- [8] Galazka Z, Irmscher K, Uecker R, Bertram R, Pietsch M, Kwasniewski A, et al. On the bulk β-Ga2O3 single crystals grown by the Czochralski method. J Cryst Growth 2014;404:184–91.
- [9] Galazka Z, Uecker R, Irmscher K, Albrecht M, Klimm D, Pietsch M, et al. Czochralski growth and characterization of β-Ga2O3 single crystals. Cryst Res Technol 2010;45(12):1229–36.
- [10] Zhang J, Li B, Xia C, Pei G, Deng Q, Yang Z, et al. Growth and spectral characterization of β-Ga2O3 single crystals. J Phys Chem Solids 2006;67(12): 2448–51.
- [11] Suzuki N, Ohira S, Tanaka M, Sugawara T, Nakajima K, Shishido T. Fabrication and characterization of transparent conductive Sn-doped β-Ga2O3 single crystal. Phys Status Solidi C 2007;4(7):2310–3.
- [12] Kuramata A, Koshi K, Watanabe S, Yamaoka Yu, Masui T, Yamakoshi S. High-quality β-Ga2O3 single crystals grown by edge-defined film-fed growth. Jpn J Appl Phys 2016;55(12):1202A2. https://doi.org/10.7567/JJAP.55.1202A2.
- [13] Zhou H, Zhang J, Zhang C, Feng Q, Zhao S, Ma P, et al. A review of the most recent progresses of state-of-art gallium oxide power devices. J Semicond 2019;40(1): 011803. https://doi.org/10.1088/1674-4926/40/1/011803.
- [14] Sasaki K, Kuramata A, Masui T, Villora EG, Shimamura K, Yamakoshi S. Device-quality β-Ga2O3 epitaxial films fabricated by ozone molecular beam epitaxy. Appl Phys Express 2012;5(3):035502.
- [15] Baldini M, Albrecht M, Fiedler A, Irmscher K, Klimm D, Schewski R, et al. Semiconducting Sn-doped β-Ga 2 O 3 homoepitaxial layers grown by metal organic vapour-phase epitaxy. J Mater Sci 2016;51(7):3650–6.
- [16] Baldini M, Albrecht M, Fiedler A, Irmscher K, Schewski R, Wagner G. Si-and Sn-doped homoepitaxial β-Ga2O3 layers grown by MOVPE on (010)-oriented substrates. ECS J Solid State Sci Technol. 2016;6(2):Q3040.
- [17] Du X, Li Z, Luan C, Wang W, Wang M, Feng X, et al. Preparation and characterization of Sn-doped β-Ga 2 O 3 homoepitaxial films by MOCVD. J Mater Sci 2015;50(8):3252–7.
- [18] Gogova D, Wagner G, Baldini M, Schmidbauer M, Irmscher K, Schewski R, et al. Structural properties of Si-doped β -Ga2O3 layers grown by MOVPE. J Cryst Growth 2014:401:665–9.
- [19] Lv Yu, Ma J, Mi W, Luan C, Zhu Z, Xiao H. Characterization of β-Ga2O3 thin films on sapphire (0001) using metal-organic chemical vapor deposition technique. Vacuum 2012;86(12):1850–4.
- [20] Sbrockey NM, Salagaj T, Coleman E, Tompa GS, Moon Y, Kim MS. Large-area MOCVD growth of Ga 2 O 3 in a rotating disc reactor. J Electron Mater 2015;44(5): 1357–60.
- [21] Alema F, Hertog B, Osinsky A, Mukhopadhyay P, Toporkov M, Schoenfeld WV. Fast growth rate of epitaxial β–Ga2O3 by close coupled showerhead MOCVD. J Cryst Growth 2017;475:77–82.
- [22] Takiguchi Y, Miyajima S. Effect of post-deposition annealing on low temperature metalorganic chemical vapor deposited gallium oxide related materials. J Cryst Growth 2017;468:129–34.
- [23] Sangiovanni DG, Gueorguiev GK, Kakanakova-Georgieva A. Ab initio molecular dynamics of atomic-scale surface reactions: Insights into metal organic chemical vapor deposition of AlN on graphene. PCCP 2018;20(26):17751–61.
- [24] dos Santos RB, Rivelino R, de Brito Mota F, Gueorguiev GK, Kakanakova-Georgieva A. Dopant species with Al-Si and N-Si bonding in the MOCVD of AlN implementing trimethylaluminum, ammonia and silane. J Phys D Appl Phys 2015; 48(29):295104. https://doi.org/10.1088/0022-3727/48/29/295104.
- [25] Chen X, Ren F, Gu S, Ye J. Review of gallium-oxide-based solar-blind ultraviolet photodetectors. Photonics Res 2019;7(4):381–415.
- [26] Onuma T, Saito S, Sasaki K, Masui T, Yamaguchi T, Honda T, et al. Valence band ordering in β-Ga2O3 studied by polarized transmittance and reflectance spectroscopy. Jpn J Appl Phys 2015;54(11):112601. https://doi.org/10.7567/ JJAP.54.112601.
- [27] Zhou H, Si M, Alghamdi S, Qiu G, Yang L, Ye PD. High-Performance Depletion/ Enhancement-ode \$\beta \$-Ga2O3 on Insulator (GOOI) Field-Effect Transistors With Record Drain Currents of 600/450 mA/mm. IEEE Electr Dev Lett 2017;38(1): 103-6.
- [28] Hwang WS, Verma A, Peelaers H, Protasenko V, Rouvimov S, (Grace) Xing H, et al. High-voltage field effect transistors with wide-bandgap β -Ga2O3 nanomembranes. Appl Phys Lett 2014;104(20):203111. https://doi.org/10.1063/1.4879800.
- [29] Matsuzaki K, Hiramatsu H, Nomura K, Yanagi H, Kamiya T, Hirano M, et al. Growth, structure and carrier transport properties of Ga2O3 epitaxial film examined for transparent field-effect transistor. Thin Solid Films 2006;496(1): 37-41
- [30] Agarwal S, Haseman MS, Khamehchi A, Saadatkia P, Winarski DJ, Selim FA. Physical and optical properties of Ce: YAG nanophosphors and transparent

- ceramics and observation of novel luminescence phenomenon. Opt Mater Expr. 2017;7(3):1055-65.
- [31] Agarwal S, Haseman MS, Leedy KD, Winarski DJ, Saadatkia P, Doyle E, et al. Tuning the Phase and Microstructural Properties of TiO2 Films Through Pulsed Laser Deposition and Exploring Their Role as Buffer Layers for Conductive Films. J Electron Mater 2018;47(4):2271–6.
- [32] Zhang Le, Wu J, Stepanov P, Haseman M, Zhou T, Winarski D, et al. Defects and solarization in YAG transparent ceramics. Photonics Res 2019;7(5):549. https:// doi.org/10.1364/PRJ.7.000549.
- [33] Selim FA, Khamehchi A, Winarski D, Agarwal S. Synthesis and characterization of Ce: YAG nano-phosphors and ceramics. Opt Mater Exp. 2016;6(12):3704–15.
- [34] Winarski D, Persson C, Selim FA. Hydrogen in insulating oxide Y 3 Al 5 O 12 strongly narrows the band gap. Appl Phys Lett 2014;105(22):221110. https://doi. org/10.1063/1.4903343.
- [35] Reda SM, Varney CR, Selim FA. Radio-luminescence and absence of trapping defects in Nd-doped YAG single crystals. Results Phys 2012;2:123–6.
- [36] Lyons JL, Steiauf D, Janotti A, de Walle Van, Chris G. Carbon as a shallow donor in transparent conducting oxides. Phys Rev Appl 2014;2(6). 064005.
- [37] Irmscher K, Galazka Z, Pietsch M, Uecker R, Fornari R. Electrical properties of β-Ga2O3 single crystals grown by the Czochralski method. J Appl Phys 2011;110 (6):063720. https://doi.org/10.1063/1.3642962.
- [38] Chikoidze E, Fellous A, Perez-Tomas A, Sauthier G, Tchelidze T, Ton-That C, et al. P-type β-gallium oxide: a new perspective for power and optoelectronic devices. Mater Today Phys 2017;3:118–26.

- [39] Ingebrigtsen ME, Kuznetsov AY, Svensson BG, Alfieri G, Mihaila A, Badstübner U, et al. Impact of proton irradiation on conductivity and deep level defects in β-Ga2O3. APL Mater 2019;7(2):022510. https://doi.org/10.1063/1.5054826.
- [40] Varley JB, Peelaers H, Janotti A, Van de Walle CG. Hydrogenated cation vacancies in semiconducting oxides. J Phys: Condens Matter 2011;23(33):334212. https://doi.org/10.1088/0953-8984/23/33/334212.
- [41] Selim F, inventor. Methods and systems for testing luminescent semiconductors. United States patent US 10,330,614. 2019 Jun 25.
- [42] Mackay DT, Varney CR, Buscher J, Selim FA. Study of exciton dynamics in garnets by low temperature thermo-luminescence. J Appl Phys 2012;112(2):023522. https://doi.org/10.1063/1.4739722.
- [43] Ji J, Boatner LA, Selim FA. Donor characterization in ZnO by thermally stimulated luminescence. Appl Phys Lett 2014;105(4):041102. https://doi.org/10.1063/ 1.4891677.
- [44] Islam MM, Rana D, Hernandez A, Haseman M, Selim FA. Study of trap levels in β-Ga2O3 by thermoluminescence spectroscopy. J Appl Phys 2019;125(5):055701. https://doi.org/10.1063/1.5066424.
- [45] Islam MM, Adhikari N, Hernandez A, Janover A, Novak S, Agarwal S, et al. Direct measurement of the density and energy level of compensating acceptors and their impact on the conductivity of n-type Ga2O3 films. J Appl Phys 2020;127(14): 145701. https://doi.org/10.1063/1.5143030.
- [46] Varney CR, Reda SM, Mackay DT, Rowe MC, Selim FA. Strong visible and near infrared luminescence in undoped YAG single crystals. AIP Adv 2011;1(4):042170. https://doi.org/10.1063/1.3671646.